Frustrated Structural Instability in Superconducting Quasi-One-Dimensional $K_2Cr_3As_3$

Keith M. Taddei,[1,*] Guangzong Xing,[2] Jifeng Sun,[2] Yuhao Fu,[2] Yuwei Li,[2] Qiang Zheng,[3] Athena S. Sefat,[3] David J. Singh,[2,†] and Clarina de la Cruz[1]

[1]*Neutron Scattering Division, Oak Ridge National Laboratory, Oak Ridge, Tennessee 37831, USA*

[2]*Department of Physics and Astronomy, University of Missouri, Missouri 65211, USA*

[3]*Materials Science and Technology Division, Oak Ridge National Laboratory, Oak Ridge, Tennessee 37831, USA*

(Received 9 May 2018; published 31 October 2018)

We present density functional theory and neutron total scattering studies on quasi-one-dimensional superconducting $K_2Cr_3As_3$ revealing a frustrated structural instability. Our first principles calculations find a significant phonon instability, which, under energy minimization, corresponds to a frustrated orthorhombic distortion. In neutron diffraction studies we find large atomic displacement parameters with anomalous temperature dependencies, which result from highly localized orthorhombic distortions of the CrAs sublattice and coupled K displacements. These results suggest a more complex phase diagram than previously assumed for $K_2Cr_3As_3$ with subtle interplays of structure, electron-phonon, and magnetic interactions.

DOI: 10.1103/PhysRevLett.121.187002

Prior to Bardeen, Cooper, and Schrieffer's theory of conventional superconductivity, several macroscopic phenomenological descriptions existed that could successfully reproduce the observed behaviors of superconductors [1–4]. It was the identification of electron-phonon coupling as the mediator of superconductivity and the subsequent microscopic theory that propelled the field forward and afforded new predictive powers [5,6]. No such universal interaction has been identified in the study of unconventional superconductors (UNSC) [7,8]. Yet in most UNSC, clear candidate interactions are manifested through a quasi-universal proximity to ordering instabilities—such as magnetism, charge-ordering, structural distortions or, as is often the case, confounding combinations of these orders [9–13]. For the most widely studied families (e.g., cuprates, iron based, heavy Fermion), a vital tool for discerning the relevance of these interactions to superconductivity has been the ability to tune through the instabilities via parameters such as pressure, charge doping, and strain [11,14,15].

Recently, a new family of possible UNSC was discovered, $A_2Cr_3As_3$ (with $A =$ Na, K, Rb, Cs), which has generated significant interest due to potentially exotic physics and provocative properties such as structural quasi-one-dimensionality (Q1D), noncentrosymmetry, Luttinger-liquid-like behavior and the transition-metal pnictide composition [16–23]. The main structural motif of CrAs double-walled subnano tubes is a fascinating contrast to the 2D transition-metal planes of the cuprates and iron-based superconductors. However, unlike its 2D brethren, the $A_2Cr_3As_3$ materials have proven difficult to tune, being unreceptive to chemical doping and robust against internal or external pressure, which only suppresses the superconducting transition temperature (T_c) [19,24].

Furthermore, while measurements of dynamic phenomena have revealed signatures of spin fluctuations, no long-range order analogous to the spin or charge density waves of the classic UNSC has been observed [25–28]. Initial findings of a possible spin-glass phase in the similar 1:3:3 stoichiometry (ACr_3As_3) have given way to findings of robust superconductivity with no static magnetism [29–31]. In the absence of clear evidence of a nearby instability, the superconducting mechanism remains elusive and conflicting suggestions have developed, ranging from spin fluctuations to conventional phonons [25,32–34]. Therefore, any evidence of instabilities could be vital to understanding this material and how it fits into the wider narrative of UNSC.

To better understand superconductivity in $K_2Cr_3As_3$ we performed first-principles calculations, which predicted a significant in-plane phonon instability with a large degeneracy resulting in a frustrated instability of the $P\bar{6}m2$ structure. As a first approach for experimental verification, we conducted a careful analysis of the atomic displacement parameters (ADPs) observing an anomalous temperature dependence which is localized to the *ab* plane. Using pair distribution function (PDF) techniques to probe the local structure, we found an orthorhombic distortion localized to single CrAs tubes. These results indicate that, in addition to the previously reported proximate magnetic instability, $K_2Cr_3As_3$ has a structural instability albeit frustrated and thus an important similarity to the wider family of UNSC [25].

Density functional theory (DFT) calculations were performed using the generalized gradient approximation, projector-augmented wave method, and the general potential linearized augmented plane-wave method with the

experimental lattice parameters (see Supplemental Material [35]) [36–40]. Neutron total scattering measurements were performed on the NOMAD time-of-flight diffractometer of Oak Ridge National Laboratory's Spallation Neutron Source and the data reduced using the instrument developed software [41,42]. The diffraction data were used (along with the data reported in Ref. [25]) for Rietveld refinements (as implemented in the GSAS and EXPGUI software suites) to model the ADPs and their temperature dependence [43–45]. For our PDF analysis, least-squares refinements were performed as implemented in PDFGUI [46,47]. Symmetry analysis was performed using ISODISTORT [48].

Initially motivated to check for a potential conventional superconducting mechanism, we performed DFT calculations to study electron-phonon coupling in $K_2Cr_3As_3$. Unexpectedly, our calculated phonon spectrum [Fig. 1(a)] predicted a substantial structural instability of the CrAs tubes—in contrast to previous work [32]. This is apparent in the negative energy optical phonon branch observed along the in-plane $\Gamma - K$, $K - M$, and $M - \Gamma$ directions (standard labels are used as in Refs. [17,18]). The existence of a negative energy phonon mode suggests a distortion to a lower symmetry structure. However, the unstable branches are nearly dispersionless in-plane, which should confound the selection of a minimum energy distortion direction. By comparison, significant dispersion is seen along the tube direction ($\Gamma - A$). We interpret this in-plane phonon energy degeneracy as representing a frustration that would work against long-range ordering in-plane.

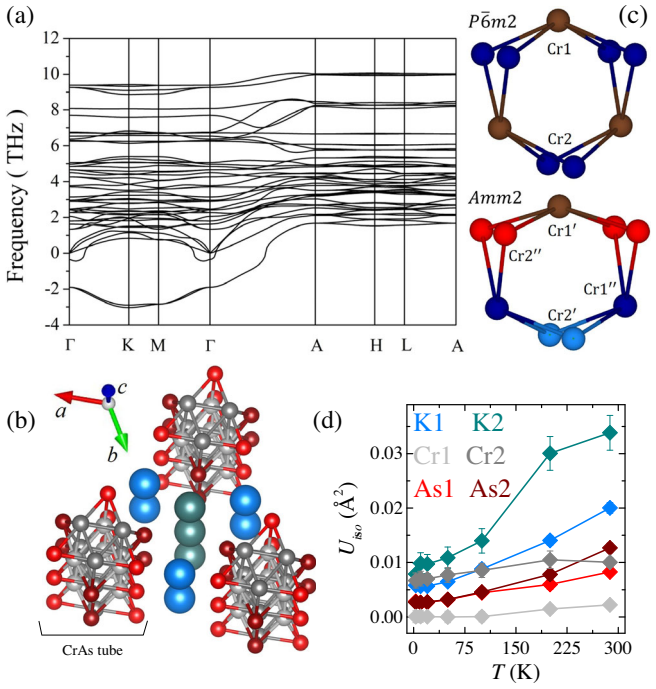

FIG. 1. Results of DFT calculations and preliminary diffraction analysis. (a) Phonon dispersions for selected high-symmetry directions through the Brillouin zone. (b) Structural model emphasizing the CrAs tubes and the threefold C_3 symmetry. (c) Initial $P\bar{6}m2$ Cr sublattice used as the input structure for DFT and the predicted $Amm2$ structure found in structural relaxation under energy minimization. (d) Temperature dependence of the atomic displacement parameters (U), from Rietveld refinements performed with diffraction data. The atom labels and color coding used in panel (d) and (b) are consistent though not with (c), where more colors were needed due to the number of sites.

To characterize the possible structural distortion, we allowed the crystallographic parameters to relax following energy minimization. We started from the reported $P\bar{6}m2$ structure [Fig. 1(b)] which consists of two inequivalent alternating stacked planes at $z = 0, \frac{1}{2}$. Each plane has unique K, Cr, and As sites with atomic labels and Wyckoff positions: [K1($3k$), Cr1($3k$), As2($3k$)] and [K2($1c$), Cr2($3j$), As1($3j$)] for $z = 0, \frac{1}{2}$, respectively. Under energy minimization we find the structure undergoes a Γ point distortion to the $Amm2$ orthorhombic symmetry due to the unstable phonon mode [Fig. 1(c)]. This breaks the $\bar{6}$ roto-inversion symmetry and splits each of the Cr1(2), As1(2), and K1 sites into two. Additionally, broken mirror symmetries allow for displacements along the (210) direction.

To check for possible evidence of this distortion in the measured properties, we calculated the density of states for both the $P\bar{6}m2$ and $Amm2$ structures. While the expected frustration of this order complicates the interpretation, we do not observe large changes that would predict significant modifications to transport properties (see Supplemental Material [35]). Therefore, we rely on diffraction studies to search for the predicted distortion. Previously, we reported the $P\bar{6}m2$ model as adequate for fits of high resolution diffraction data [25]. This limits physical manifestations of the DFT results, indicating either a small (resolution limited) upper limit to the distortion magnitude or a local distortion model. The latter agrees with our predicted lattice frustration encouraging a study of the local structure. Therefore, we used neutron diffraction data collected to high scattering angle to model the isotropic ADPs (U_{iso}) via standard Rietveld refinement techniques in the $P\bar{6}m2$ structure. ADPs measure the mean square variance in atomic positions and can give evidence of lattice disorder via large values or temperature independent behavior [49–52].

The resulting temperature dependent ADPs are shown in Fig. 1(d). Comparing our values to related materials we find ADPs significantly larger than in the structurally related (and stable) Q1D Chevrel phases and larger than those reported in the iron-based superconductors, which are famous for their local nematicity [53–55]. Moreover, the values obtained for the K site are similar to the Einstein "rattler" behavior seen in thermoelectric materials [52,56]. To this latter comparison, we similarly observe significant residual U_{iso} at 2 K on the K2 site. The Cr2 site not only exhibits a relatively large residual ADP but also shows little temperature dependence between 300 and 2 K. In contrast, the As1, As2, and Cr2 sites show Debye-Waller

type behavior, tending towards low values as $T \to 0$ K. The temperature dependence of the former three sites, indicates ADPs not exclusively driven by standard thermal effects.

To better characterize the structural effects causing the large ADPs, we performed PDF analysis, which takes the Fourier transform of the normalized diffraction pattern to generate the real space atomic correlation function $G(r)$. Fitting the transformed data shifts the features of the fit to direct atom-atom spacings (measured by r in Å), rather than crystallographic symmetry. Therefore, it allows for the modeling of the local structure through least-squares techniques [46,47].

Figure 2(a) shows $G(r)$ for $K_2Cr_3As_3$ collected at 2 K and a corresponding fit using the symmetry constraints of the $P\bar{6}m2$ structure. Here, we model only the low-r region of 2.1–20 Å, which covers approximately the first two unit cells of the hexagonal structure and therefore accentuate the local structure in the fit (see Supplemental Material [35]). We start with the symmetry constraints of $P\bar{6}m2$ to refine

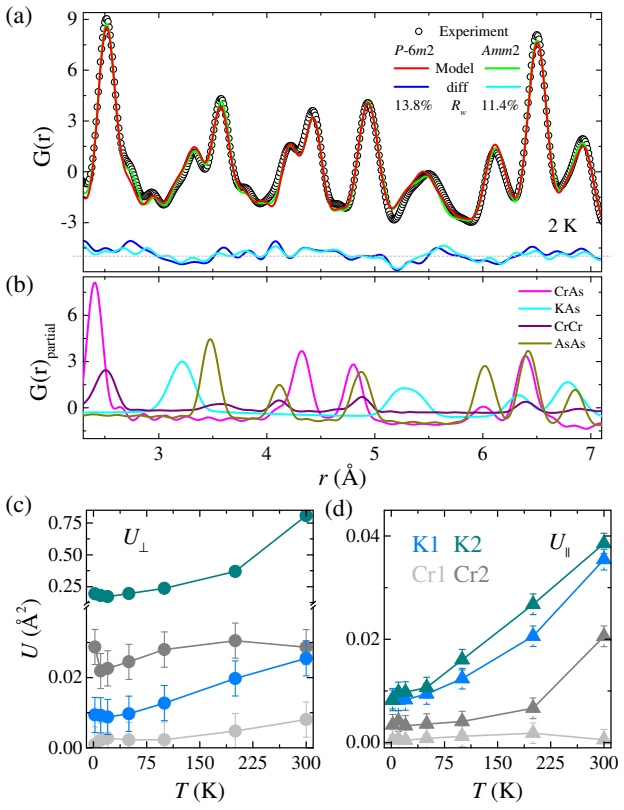

FIG. 2. Results of PDF analyses. (a) Observed 2 K $G(r)$ (where r is a real-space distance measured in Å), plotted with the $G(r)$'s calculated from the $P\bar{6}m2$ and $Amm2$ Rietveld refined models. Difference curves (observed–calculated) for each model are shown with an arbitrary offset. (b) Partial PDF showing the K-As, Cr-As, Cr-Cr, and As-As correlation functions for a $P\bar{6}m2$ fit. Anisotropic U parameter determined from PDF analysis for (c) ab plane ($U_\perp$) and (d) lattice c direction ($U_\parallel$). ADPs for As1 (2), which show unremarkable temperature dependence, are not shown in panels (c) and (d) to provide visual clarity.

our discussion of the ADPs, which are more directly modeled in $G(r)$ as peak widths. Motivated by the coplanar arrangement of the atomic sites, we treat the ADPs anisotropically with in-plane ($U_\perp$) and out-of-plane ($U_\parallel$) components [Figs. 2(c) and 2(d)]. This analysis reveals that the large ADPs of K2 and Cr2 shown in Fig. 1(d) arise from $U_\perp$, which displays both behaviors. Meanwhile, $U_\parallel$ is mostly Debye-Waller-like [Fig. 2(d)]. The $U_\perp$(2K) values are quite large compared to similar materials and indicate possible local disorder of the K2 and Cr2 sites within the ab plane as expected for an $Amm2$ type distortion [53,54].

Beyond large ADPs, we note the generally poor fit of the $P\bar{6}m2$ model to the low-r PDF data [Fig. 2(a)]. Several features are missed, and intensities mismatched which result in a relatively large fit residual R_w (for reference a crystalline standard results in $R_w \sim 10\%$). Despite the complicated CrAs tube geometry with many similar [overlapping in $G(r)$] bond lengths [Fig. 2(b)], a series of peaks ($r = 2.6$ and 5.4 Å) can be identified which are missed by the $P\bar{6}m2$ model [Fig. 2(a)]. This suggests additional atom-atom distances not allowed in the average structure. The anomalously large ADPs of K2 and Cr2 result from the model attempting to fit these extra correlation lengths—broadening the peaks and reducing the peak intensity to account for the smaller coordination number. If we model with ADP values of similar materials and structures (i.e., with smaller ADPs), the intensity mismatch is exacerbated, supporting this interpretation [53,54].

To account for these features, we attempted modeling of our PDF data allowing for atomic displacements consistent with the maximal symmetry subgroups of $P\bar{6}m2$—including $Amm2$. Of these, we focus on the $Amm2$ model as the highest symmetry distortion capable of improving our PDF fit (see Supplemental Material [35]). As in the $P\bar{6}m2$ refinements, at first we refined the atomic sites with the symmetry constraints of the space group. Additional constraints were applied to ensure the same number of refinable parameters in each model—an important condition to prevent overparametrization of the limited r range considered.

As discussed, the $Amm2$ model splits the $3k$ and $3j$ Wyckoff sites into two independent sites each and thus breaks the degeneracy of several bond lengths. In doing so, the $Amm2$ structure can model the previously missed peaks and reduces the R_w parameter from 13.8% to 11.4% [Fig. 2(a)]. Furthermore, these newly allowed displacements reduce the U for K2 from 0.30 to 0.03 Å^2 (for first unit cell r range). This indicates the large ADPs found in the $P\bar{6}m2$ model result from the model attempting to fit split peaks.

The fitted $Amm2$ structure is shown in Fig. 3. The main differences from $P\bar{6}m2$ [Fig. 1(b)] are a large displacement of the K2 site along the orthorhombic (210) direction and the breaking of the CrAs tubes' C_3 rotational symmetry.

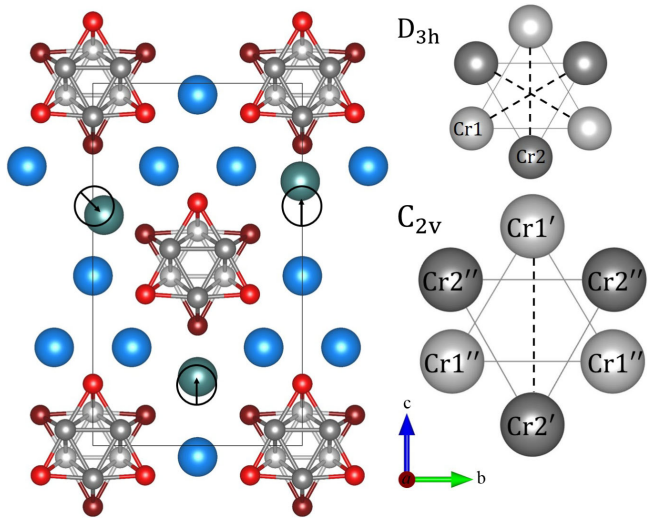

FIG. 3. (left) $Amm2$ structure determined in low-r PDF fits, the results of the three site K2 refinement are shown, with black circles and arrows marking the $P\bar{6}m2$ K2 position and the direction of the displacement, respectively. This reveals a lack of displacement direction correlation between neighboring K2's. (right) Symmetry of the Cr tubes in the $P\bar{6}m2$ and $Amm2$ space groups (point groups D_{3h} and C_{2v}, respectively) with mirror planes represented by dashed lines.

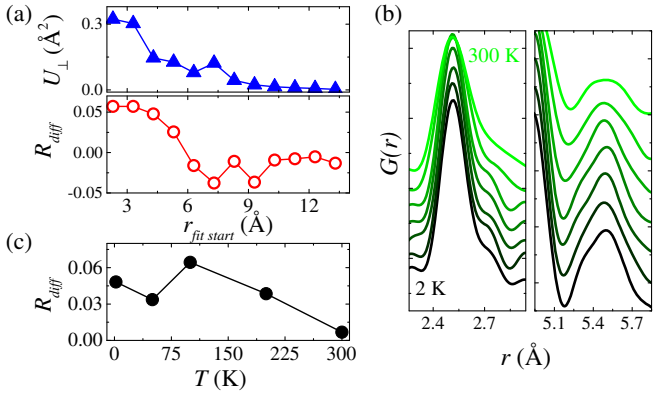

FIG. 4. (a) $U_\perp$ and the normalized R factors (R_{diff}) as functions of starting r (r_{fitstart}) for boxcar PDF fits using $Amm2$ and $P\bar{6}m2$ symmetry constraints. (b) Waterfall plots showing temperature dependence of the $G(r)$ 2.7 and 5.4 Å peaks. Patterns collected at 2(black), 10, 20, 50, 150, 200, and 300 K (green). (c) Temperature dependence of R_{diff} for low-r PDF fits.

Previous DFT work has suggested the position of the K ions couple to the Cr-Cr bonding via the electron distribution [17,26,33]. Because of the bonding (antibonding) nature of the Cr-Cr(Cr-As) bonds, the displacement of K2 towards the CrAs tube should decrease (increase) the respective bond lengths or vice versa [17]. This is what we see as the triply degenerate 2.66 Å Cr2-Cr2 bond breaks into a 2.55 Å and two 2.65 Å bonds and the 2.49 Å Cr2-As1 bond breaks into a 2.58 Å and two 2.51 Å bonds—the shorter Cr-Cr and longer Cr-As corresponding to the Cr closest to the displaced K (Fig. 3).

The analysis of the standard diffraction and PDF data indicate significant local distortions that are uncorrelated over long distances, averaging to $P\bar{6}m2$. To investigate the scale of this transition, boxcar fits of the PDF data were performed by choosing a window size ($\Delta r \sim 9$ Å) and then sliding the starting r value (r_{fitstart}) of the fit range to increasing r. In this way, the analysis can be shifted from the local structure to the approximate averaged structure and the fit residuals of the $P\bar{6}m2$ and $Amm2$ models can be compared over different correlation lengths. This is possible because $G(r)$ at large r approximates the average structure by invoking larger coordination distances which inherently average out local effects.

The normalized difference of R_w [$R_{\mathrm{diff}} = 2 * (R_{\mathrm{orth}} - R_{\mathrm{hex}})/(R_{\mathrm{orth}} + R_{\mathrm{hex}})$] from boxcar fits is shown in Fig. 4(a). For the lowest r_{fitstart}, the orthorhombic model results in significantly improved R_{diff}. However, by $r_{\mathrm{fitstart}} = 6.3$ Å the hexagonal model produces nearly identical R_w to the orthorhombic model—indicating that by 6.3 Å modeling with ADPs is as good as with the orthorhombic distortion. At higher r_{fitstart}, R_{diff} settles to zero. Similarly, we can fit $U_\perp$ as a function of r_{fitstart}, [Fig. 4(a)] revealing a quick drop-off of the K2 ADP which approaches the value found in standard diffraction analysis ($U_\perp \approx 0.01$ Å^2) by $r_{\mathrm{fitstart}} = 9$ Å.

These distance scales are approximately the size of the CrAs tubes but smaller than the intertube spacing (~10 Å) indicating the distortion is essentially uncorrelated between neighboring unit cells. We note that each CrAs tube has C_3 rotational symmetry and therefore can distort along any of three directions. When $r_{\mathrm{fitstart}} = 6.3$ Å correlations over 15 Å are considered including the next nearest CrAs tube and 8 in-plane K2 correlations for every CrAs tube and the orthorhombic distortion averages to the $P\bar{6}m2$ structure. This is consistent with inherent frustration indicated by the degeneracy of the relevant phonon mode in the $k_z = 0$ plane. In fact, models using $Pmm2$ symmetry which create two distinct CrAs tubes, further reduce R_w. However, $Pmm2$ produces more refinable parameters and direct comparisons of R_w with the $P\bar{6}m2$ model are more ambiguous. We therefore base our conclusions on the $Amm2$ distortion.

To corroborate this length scale, we performed PDF refinements with the symmetry constraints of the K2 sites in the $Amm2$ model removed. This introduces fewer additional parameters than lower symmetry space groups while still allowing us to check the independence of the tubes. This model resulted in uncorrelated displacements between the K2 sites (Fig. 3) which nonetheless remained along the mirror planes of the C_3 symmetry. We suggest the distortion happens randomly from CrAs to the CrAs tube. Such disorder would give rise to the observed average structure and a large in-plane ADP for the K2 and Cr2 sites over long correlation lengths.

Identifying whether these distortions are static or dynamic is of great interest to their relevance to superconductivity. However, the technique of neutron total scattering integrates over finite energy transfer and the resulting PDF pattern includes dynamic effects with the energy scale of several meV (or 10^{-13} s) [55]. The temperature dependence of the distortion can instead be used as an indirect probe for the timescale of the correlations, with temperature independence being expected of static effects. Figure 4(b) shows the two clearest split peaks between 2 and 300 K. In both cases the distortion is seen to persist to 300 K—albeit with considerable broadening. We also performed fit comparisons between the two models over the measured temperature range [Fig. 4(c)], and found the orthorhombic model to always produce reduced R_w. This temperature dependence is more indicative of a static distortion than of fluctuations. However, further studies of the lattice dynamics are needed to clarify this important distinction.

Our results indicate that $K_2Cr_3As_3$ is susceptible to an orthorhombic distortion that is frustrated by a nearly degenerate in-plane dispersion of the relevant phonon mode. We find distortions of the CrAs tubes and coupled K site displacements consistent with a DFT predicted *Amm*2 symmetry lowering. However, no significant correlation from unit cell to unit cell occurs, preventing long-range orthorhombic order. That $K_2Cr_3As_3$ has such an instability is significant to the material's position within the wider family of UNSC. Such a lattice distortion more clearly places it on similar footing with the cuprate and iron-based materials which tend to exhibit structural and magnetic instabilities.

This manuscript has been authored by UT-Battelle, LLC under Contract No. DE-AC05-00OR22725 with the U.S. Department of Energy. The United States Government retains and the publisher, by accepting the article for publication, acknowledges that the United States Government retains a non-exclusive, paid-up, irrevocable, world-wide license to publish or reproduce the published form of this manuscript, or allow others to do so, for United States Government purposes. The Department of Energy will provide public access to these results of federally sponsored research in accordance with the DOE Public Access Plan. A portion of this research used resources at the High Flux Isotope Reactor and the Spallation Neutron Source, a U.S. Department of Energy (DOE) Office of Science User Facility operated by the Oak Ridge National Laboratory. The research is partly supported by the U.S. DOE, Office of Science, Basic Energy Sciences (BES), Materials Science and Engineering Division. Work at the University of Missouri is supported by the U.S. DOE, BES, Award No. DE-SC0019114. The authors thank B. A. Frandsen, M. McDonnell, and T.-M. Usher-Ditzian for guidance with PDFGUI and J. Neuefeind for help with data collection on NOMAD.

*Corresponding author.
taddeikm@ornl.gov
†Corresponding author.
singhdj@missouri.edu

[1] J. Bardeen, L. N. Cooper, and J. R. Schrieffer, Phys. Rev. **108**, 1175 (1957).
[2] M. R. Schafroth, Phys. Rev. **96**, 1149 (1954).
[3] F. London and H. London, Proc. R. Soc. A **149**, 71 (1935).
[4] V. I. Ginzburg, J. Exp. Theor. Phys. **2**, 589 (1956).
[5] V. Ginzburg, Phys. Usp. **40**, 407 (1997).
[6] N. W. Ashcroft, Phys. Rev. Lett. **21**, 1748 (1968).
[7] G. R. Stewart, Adv. Phys. **66**, 75 (2017).
[8] M. R. Norman, Science **332**, 196 (2011).
[9] D. Basov and A. Chubukov, Nat. Phys. **7**, 272 (2011).
[10] S. Avci, O. Chmaissem, E. A. Goremychkin, S. Rosenkranz, J.-P. Castellan, D. Y. Chung, I. S. Todorov, J. A. Schlueter, H. Claus, M. G. Kanatzidis, A. Daoud-Aladine, D. Khalyavin, and R. Osborn, Phys. Rev. B **83**, 172503 (2011).
[11] A. Chubukov, Annu. Rev. Condens. Matter Phys. **3**, 57 (2012).
[12] R. M. Fernandes, A. V. Chubukov, and J. Schmalian, Nat. Phys. **10**, 97 (2014).
[13] B. D. White, J. D. Thompson, and M. B. Maple, Physica (Amsterdam) **514C**, 246 (2015).
[14] P. Monthoux, D. Pines, and B. Lonzarich, Nature (London) **450**, 1177 (2007).
[15] S. Lederer, Y. Schattner, E. Berg, and S. A. Kivelson, Proc. Natl. Acad. Sci. U.S.A. **114**, 4905 (2017).
[16] J.-K. Bao, L. Li, Z.-T. Tang, Y. Liu, Y.-K. Li, H. Bai, C.-M. Feng, Z.-A. Xu, and G.-H. Cao, Phys. Rev. B **91**, 180404 (2015).
[17] P. Alemany and E. Canadell, Inorg. Chem. **54**, 8029 (2015).
[18] H. Jiang, G. Cao, and C. Cao, Sci. Rep. **5**, 16054 (2015).
[19] Z. Wang, W. Yi, Q. Wu, V. A. Sidorov, J. Bao, Z. Tang, J. Guo, Y. Zhou, S. Zhang, H. Li, Y. Shi, X. Wu, L. Zhang, K. Yang, A. Li, G. Cao, J. Hu, L. Sun, and Z. Zhao, Sci. Rep. **6**, 37878 (2016).
[20] Y. Liu, J.-K. Bao, H.-K. Zuo, A. Ablimit, Z.-T. Tang, C.-M. Feng, Z.-W. Zhu, and G.-H. Cao, Sci. China: Phys., Mech. Astron. **59**, 657402 (2016).
[21] Y. Zhou, C. Cao, and F.-C. Zhang, Sci. Bull. **62**, 208 (2017).
[22] M. D. Watson, Y. Feng, C. W. Nicholson, C. Monney, J. M. Riley, H. Iwasawa, K. Refson, V. Sacksteder, D. T. Adroja, J. Zhao, and M. Hoesch, Phys. Rev. Lett. **118**, 097002 (2017).
[23] Q.-G. Mu, B.-B. Ruan, B.-J. Pan, T. Liu, J. Yu, K. Zhao, G.-F. Chen, and Z.-A. Ren, Phys. Rev. Mater. **2**, 034803 (2018).
[24] G. Cao, J.-K. Bao, Z.-T. Tang, Y. Liu, and H. Jiang, Philos. Mag. **97**, 591 (2017).
[25] K. M. Taddei, Q. Zheng, A. S. Sefat, and C. de la Cruz, Phys. Rev. B **96**, 180506 (2017).
[26] H. Z. Zhi, T. Imai, F. L. Ning, J.-K. Bao, and G.-H. Cao, Phys. Rev. Lett. **114**, 147004 (2015).
[27] J. Yang, Z. T. Tang, G. H. Cao, and G.-q. Zheng, Phys. Rev. Lett. **115**, 147002 (2015).
[28] H. Zhi, D. Lee, T. Imai, Z. Tang, Y. Liu, and G. Cao, Phys. Rev. B **93**, 174508 (2016).
[29] C. Cao, H. Jiang, X.-Y. Feng, and J. Dai, Phys. Rev. B **92**, 235107 (2015).

[30] Q.-G. Mu, B.-B. Ruan, B.-J. Pan, T. Liu, J. Yu, K. Zhao, G.-F. Chen, and Z.-A. Ren, Phys. Rev. B **96**, 140504 (2017).
[31] T. Liu, Q.-G. Mu, B.-J. Pan, B.-B. R. J. Yu, K. Zhao, G.-F. Chen, and Z.-A. Ren, Europhys. Lett. **120**, 27006 (2018).
[32] A. Subedi, Phys. Rev. B **92**, 174501 (2015).
[33] X.-X. Wu, C.-C. Le, J. Yuan, H. Fan, and J.-P. Hu, Chin. Phys. Lett. **32**, 057401 (2015).
[34] L.-D. Zhang, X.-X. Wu, H. Fan, F. Yang, and J.-P. Hu, Europhys. Lett. **113**, 37003 (2016).
[35] See Supplemental Material at http://link.aps.org/supplemental/10.1103/PhysRevLett.121.187002 for further discussions related to data collection, data reduction, Rietveld refinement methodology, symmetry analysis, structural modeling, and details of the density functional theory calculations.
[36] J. P. Perdew, K. Burke, and M. Ernzerhof, Phys. Rev. Lett. **77**, 3865 (1996).
[37] G. Kresse and D. Joubert, Phys. Rev. B **59**, 1758 (1999).
[38] G. Kresse and J. Furthmüller, Phys. Rev. B **54**, 11169 (1996).
[39] D. Singh and L. Nordström, *Planewaves, Pseudopotentials and the LAPW Method*, 2nd ed. (Springer, Berlin, 2006).
[40] A. Togo and I. Tanaka, Scr. Mater. **108**, 1 (2015).
[41] M. T. McDonnell, D. P. Olds, K. L. Page, J. C. Neufeind, M. G. Tucker, J. C. Bilheux, W. Zhou, and P. F. Peterson, Acta Crystallogr. Sect. A **73**, a377 (2017).
[42] J. Neuefeind, M. Feygenson, J. Carruth, R. Hoffmann, and K. K. Chipley, Nucl. Instrum. Methods **287**, 68 (2012).
[43] B. H. Toby, Powder Diffr. **21**, 67 (2006).
[44] A. Larson and R. Von Dreele, Los Alamos National Laboratory, Los Alamos, NM Report No. LAUR, 86, 2004.
[45] R. B. Von Dreele, J. D. Jorgensen, and C. G. Windsor, J. Appl. Crystallogr. **15**, 581 (1982).
[46] C. Farrow, P. Juhas, J. Liu, D. Bryndin, E. Boin, J. Bloch, T. Proffen, and S. Billinge, J. Phys. Condens. Matter **19**, 335219 (2007).
[47] T. Proffen and S. J. L. Billinge, J. Appl. Crystallogr. **32**, 572 (1999).
[48] B. J. Campbell, H. T. Stokes, D. E. Tanner, and D. M. Hatch, J. Appl. Crystallogr. **39**, 607 (2006).
[49] D. W. J. Cruickshank, Acta Crystallogr. **9**, 747 (1956).
[50] J. Dunitz, V. Schomaker, and K. Trueblood, J. Phys. Chem. **92**, 856 (1988).
[51] B. Sales, B. Chakoumakos, D. Mandrux, and J. Sharp, J. Solid State Chem. **146**, 528 (1999).
[52] B. C. Sales, B. C. Chakoumakos, R. Jin, J. R. Thompson, and D. Mandrus, Phys. Rev. B **63**, 245113 (2001).
[53] P. Gall, T. Guizouarn, M. Potel, and P. Gougeon, J. Solid State Chem. **220**, 213 (2014).
[54] BaFe2As2 crystal structure: Datasheet from "Pauling file multinaries edition—2012" in springermaterials, (2006), copyright 2016 Springer-Verlag Berlin Heidelberg & Material Phases Data System (MPDS), Switzerland & National Institute for Materials Science (NIMS), Japan.
[55] B. A. Frandsen, K. M. Taddei, M. Yi, A. Frano, Z. Guguchia, R. Yu, Q. Si, D. E. Bugaris, R. Stadel, R. Osborn, S. Rosenkranz, O. Chmaissem, and R. J. Birgeneau, Phys. Rev. Lett. **119**, 187001 (2017).
[56] B. C. Sales, B. C. Chakoumakos, and D. Mandrus, Phys. Rev. B **61**, 2475 (2000).